Biomimetic Carbon Nanotube Films with Gradient Structure and Locally Tunable Mechanical Property

Zhiqiang Lin, Xuchun Gui, Zhiping Zeng, Binghao Liang, Wenjun Chen, Ming Liu, Yuan Zhu, Anyuan Cao,* and Zikang Tang*

Naturally existing materials often acquire unique functions by adopting a gradient structure with gradual change in their microstructure and related properties. Imparting such an elegant structural control into synthetic materials has been a grand challenge in the field. Here, the concept of gradient structure into macroscopic carbon nanotube (CNT) films is employed and the CNT arrangement from well-aligned array to completely random distribution, in a continuous and smooth way, is changed. Gradient films with tailored aligned-to-random transition rate or multilevel hierarchical structures with repeated transition have been fabricated. Local deformation and mechanical properties are directly related to the arrangement of CNTs and can be tailored by Herman's orientation factor; in particular, the elastic modulus and stiffness span over several orders of magnitude from aligned to random regions within a single monolithic film. Controlled synthesis of macroscopic CNT gradient structures with tunable mechanical properties opens a potential route toward manufacturing biomimetic functional materials with locally optimized design.

1. Introduction

Biological materials with gradient structures and locally tuned mechanical properties are self-protecting, functional strategy to achieve unusual mechanical properties.[1–4] These structures exist in nature widely, both in animals and plants. For instance, the teeth of many animals exhibit a bilayer structure that includes a remarkable surface hardness to withstand mastication friction and a high toughness in the inner layer to resist crack propagation.[3] Similarly, fish armour combines distinctly multiple reinforcing composite layers, which were connected by graded junctions between ganoine–dentine layers.[2] It is suggested that the gradient junction with a gradual spatial change in properties could significantly promote load transfer and stress redistribution, thus preventing delamination between dissimilar layers.[2] Such gradient mechanical properties of biological materials have inspired scientists to construct biomimetic structures by synthetic materials,[1–5] including alloy, polymer, and composite.[3,6–8] For example, a biomimetic composite with local elastic moduli tunable over five orders of magnitude has been prepared by site-specific reinforcement and tailoring the concentration of reinforcing platelets.[3] The variable mineral content on nonwoven mat of nanofibers could result in a spatial gradient in the stiffness of the scaffold.[7] In addition, in typical composite structures, the sharp interfaces where premature failure often occurs due to the stress concentration, have been replaced by a gradient interface that produces a smooth transition, resulting in higher performance of the materials.[4,8]

Carbon nanotubes (CNTs) with excellent mechanical properties have been widely used to assemble 3D bioinspired structures, including aligned arrays, lightweight highly porous sponges, and aerogels.[9–15] For example, CNT arrays with strong adhesion force to solid surface were used to create gecko-foot-mimetic dry adhesives.[10] For 1D nanostructures such as CNTs, their alignment is the most important structural factor that determines the mechanical property of CNT-based materials. As a result, macroscopic CNT structures show a wide range of strengths and moduli depending on their configuration (how CNTs are assembled).[9,16–18] Vertically aligned CNT arrays, an anisotropic configuration, show compressive moduli ranging from several MPa to tens of GPa along the axis direction.[9,16,17] In comparison, isotropic aerogels and sponges consisting of randomly overlapped CNTs are typically very soft (with lowest moduli on the order of kPa).[11–14,19] Recently, there have been a number of studies in exploring how to synthesize vertically aligned multiwalled or single-walled nanotube arrays with tailored configuration. Their results suggested that the degree of alignment depended on the catalyst distribution,[20,21] while disturbance of carbon source and catalyst precursor during

Z. Lin, Prof. X. Gui, Z. Zeng, B. Liang, W. Chen, M. Liu, Prof. Y. Zhu, Prof. Z. Tang
State Key Lab of Optoelectronic Materials and Technologies
School of Physics and Engineering
Sun Yat-sen University
Guangzhou 510275, P. R. China
E-mail: guixch@mail.sysu.edu.cn
Prof. A. Cao
Department of Materials Science and Engineering
College of Engineering
Peking University
Beijing 100871, P. R. China
E-mail: anyuan@pku.edu.cn
Prof. Z. Tang
Institute of Applied Physics and Materials Engineering
University of Macau
Avenida da Universidade
Taipa, Macau, China

DOI: 10.1002/adfm.201503341

the growth period could induce structural heterogeneity such as the formation of horizontal bands across the array.[22–25] Despite those efforts, controlled synthesis of gradient CNT structures that could mimic biological systems remains a huge challenge, and related properties of gradient CNTs are still unknown.

Here, we report a method to fabricate biomimetic gradient CNT films in which the CNT arrangement changes smoothly from well aligned array to random spatial distribution. Such effective and large-degree control of the CNT configuration within a single macroscopic monolith has not been realized before. The resulting gradient structure exhibits elastic moduli and stiffness values spanning over several orders of magnitude from aligned to random regions. We have performed in situ and dynamic mechanical tests to investigate the compressive behavior of gradient structure CNTs and interpreted the relationship between local deformation and the degree of CNT arrangement quantitatively. In particular, we find that Herman's orientation factor (HOF) is an important factor that can tailor local mechanical properties across a wide range.

2. Results and Discussion

Gradient CNT samples were fabricated by a floating catalyst chemcial vapor deposition (CVD) process that combines the recipes for growing aligned CNT arrays and random sponges as reported previously.[11,26] Specifically, liquid carbon source (xylenes and dichlorobenzene) were mixed in situ with changing concentration to induce structural transition during CVD (see the Experimental Section for details and Figure S1 in the Supporting Information). Monolithic structures with a size of $10 \times 4 \times 1$ mm^3 were synthesized and peeled off from substrate as freestanding films (**Figure 1**a). From the side, the color changes from relatively bright in the top part to relatively dark approaching the bottom (Figure 1b). Due to different light reflectivities,[27] CNTs in aligned arrangement usually appear brighter (grey color) while random arrangement looks darker. Thus the color change indicates the formation of gradient structures containing both aligned and random regions along the thickness direction of the film. The thickness of gradient structure portion in the CNT film can be tailored but not limited in the range of 200–400 μm (two samples shown in Figure 1b). The gradient CNT also could be repeated to form multilevel hierarchical structures (illustrated in Figure 1c). Many natural materials possess such kind of structure.[1,28] For example, bamboos have a graded porous structure (with changing pore size) at the cross section that is responsible for enhanced stability under different forces from nature (Figure 1d).[29]

Morphology evolution in the gradient CNT films was characterized by scanning electron microscopy (SEM). It can be

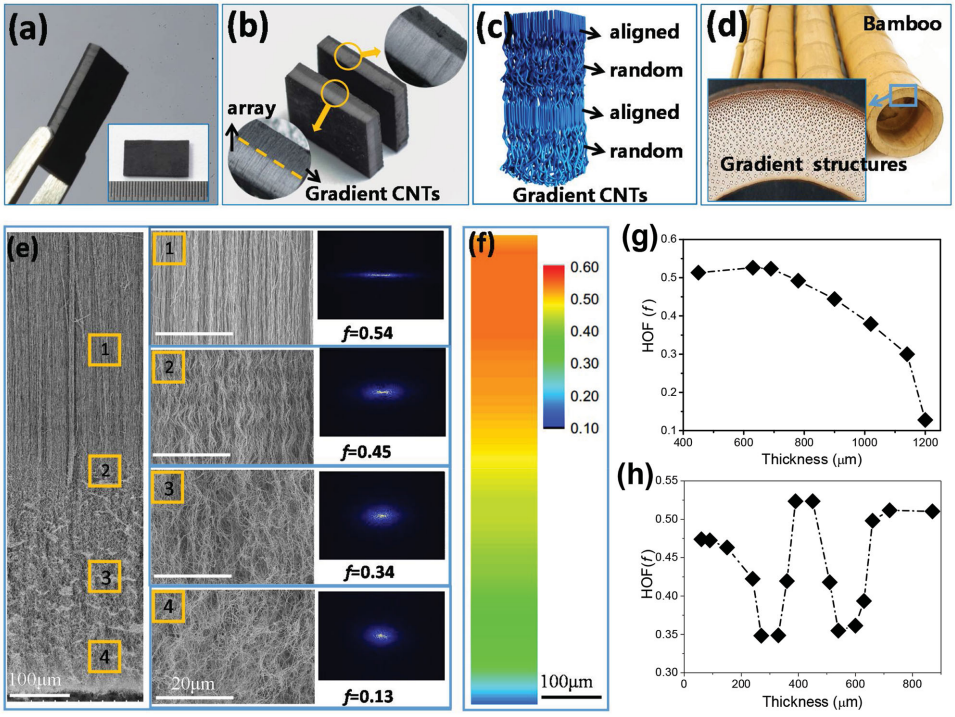

Figure 1. Gradient CNT films. a) An as-grown gradient CNT film with a size of $10 \times 4 \times 1$ mm^3. b) Two gradient CNT films with different structure transition rates. The CNT films include two portions: CNT array and gradient CNTs. The total thickness of the CNT film is about 1 mm for both, but the gradient structure portion is ≈200 and 400 μm, respectively. The darker color portion in the films has a gradient structure, and the brighter grey portion consists of aligned CNTs. c) Illustration of a gradient CNT film with a multi-level periodic hierarchical structure. d) Picture of bamboo with a gradient porous structure. e) SEM images of a gradient CNTs showing that the orientation of CNTs gradually and continuously transits from aligned (position 1) to random (position 4). After FFT of the SEM images, we obtain diffraction patterns of each position, which change from linear to circular, and the corresponding f values change from 0.54 to 0.13, starting from position 1 down to position 4. f) 2D mapping of f values for the gradeint region in (e). g) Continuous changing of f values along the thickness of gradient CNT film. h) Periodical, repeated change of f values in a multilevel hierarchical gradient film.

seen that the CNT arrangement gradually changes from well aligned to random along the thickness direction at the cross section (Figure 1e). Initially, only one carbon source (xylenes) was injected into CVD furnace, and an aligned CNT array was grown as the top portion. After that, adding the other carbon source (dichlorobenzene) disturbed aligned growth and caused loss of initial alignment. Approaching the bottom portion (final stage of growth), the CNTs were completely random like the typical morphology of CNT sponges reported by our group.[11] Although the morphology changed significantly from the top to the bottom portion, there was no obvious interface present, indicating the formation of gradient structure with smooth transition. This is because CNTs grew continuously across the gradient structure, while the only change was their reduced alignment with increasing dichlorobenzene concentration. The influence of dichlorobenzene on the arrangement of CNTs is ascribed to the chlorine-containing precursors which can provide the Cl to combine with hydrogen radicals during CVD.[30] The low H radical's contented condition is favorable to form the disorder CNTs with thin-walled CNTs.[11,31] Transmission electron microscopy (TEM) examination revealed that CNTs in both the aligned and random portion had similar diameters (proving uninterrupted growth), and also some new thin-walled nanotubes in the random region due to the introduction of dichlorobenzene (Figure S2, Supporting Information). Such continuous structural transition is different from the tandem array–sponge composite where a sharp interface exists.[26]

After fast Fourier transform (FFT) of the SEM images, we obtained the CNT arrangment information in a reciprocal space (right row of Figure 1e). From the top to bottom, the FFT images gradually transform from linear to circular as the structure shifts from ordered to random. HOF (f) calculated based on the FFT images (see the Experimental Section) was used to quantitatively describe the CNTs orientation. The f value in the aligned region equals to 0.54, consistent with other aligned multiwalled nanotube arrays (f = 0.55)[24,32,33] and lower than the superaligned single-walled nanotube forests (f = 0.85).[20] The f value gradually decreases across the gradient structure until 0.13 at the bottom of the film (Figure 1g), meaning a very random arrangement and comparable to single-walled CNT sponge (f = 0.13).[14,20] Low arrangment region (lower f value) also shows high structure defects in the Raman spectra. The intensity ratio of G peak to D peak (I_G/I_D) also gradually decrease with the decreasing of f value in the gradient CNTs (Figure S4, Supporting Information). 2D mapping of f value shows a gradient structure in the vertical direction and an isotropic structure in the horizontal plane of the film (Figure 1f). We also fabricated multilevel gradient structures in which CNTs changed from aligned to random and then from random to aligned, with f values decreasing and increasing alternatively within a certain range (0.34–0.52) (Figure 1h; Figure S4, Supporting Information). Although it was found that the arrangement of CNT in CNT arrays also change from disordered to aligned, this transformation is slight and irreversible, resulted from the self-organization of CNTs due to crowding effect (Figure S5, Supporting Information).

During CVD, the instant concentration of dichlorobenzene (C_{db}) added into the mixed carbon source was increasing continuously, and this concentration determined the morphology of growing CNTs. Under our conditions, a C_{db} range of 10%–50% was suitable for forming gradient structure; the f values decreased from 0.55 to 0.13 when the C_{db} increased from 10% to 50% (**Figure 2**a). When the C_{db} exceeded 30%, the gradient structure continued to grow at the bottom part, but another layer of random sponge would form on top of the

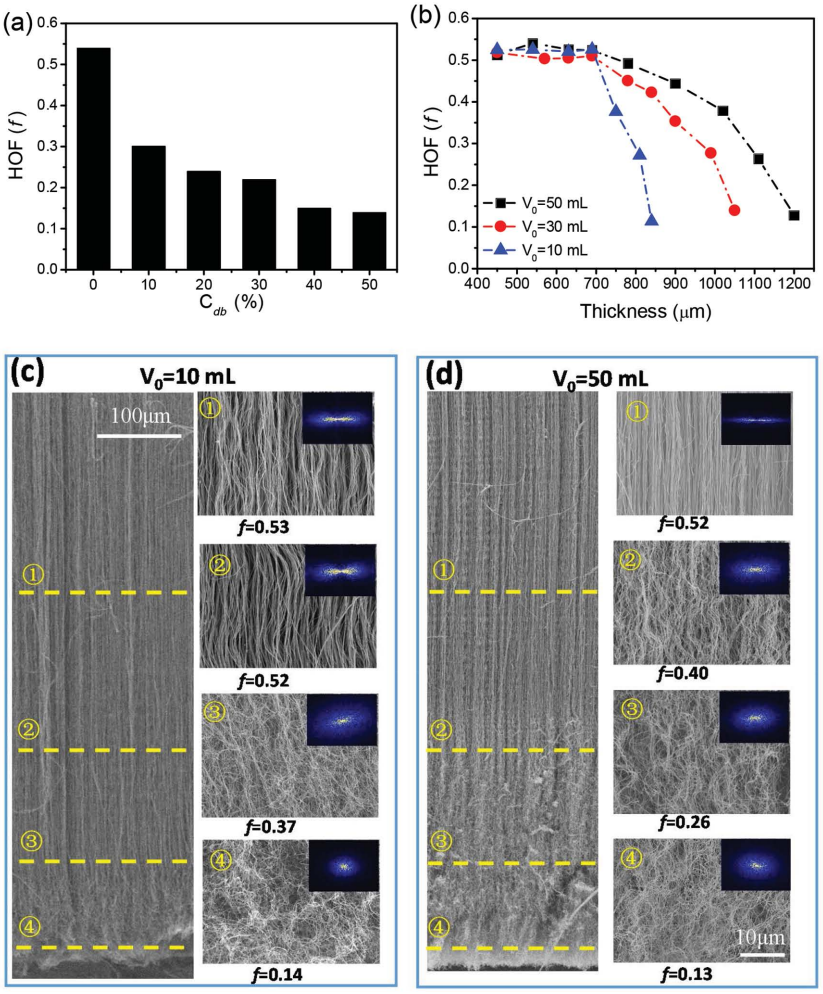

Figure 2. Tailoring structural transition rates of the gradient CNT films. a) f values of the gradient CNTs synthesized by different dichlorobenzene concentrations (C_{db}) in the carbon source solution. b) f values of gradient CNT samples synthesized with different initial volumes of xylene (V_0), showing an increase of the transition rate with lower V_0. c,d) SEM images, FFT patterns and f values of two samples synthesized with a xylene volume of 10 and 50 mL, respectively.

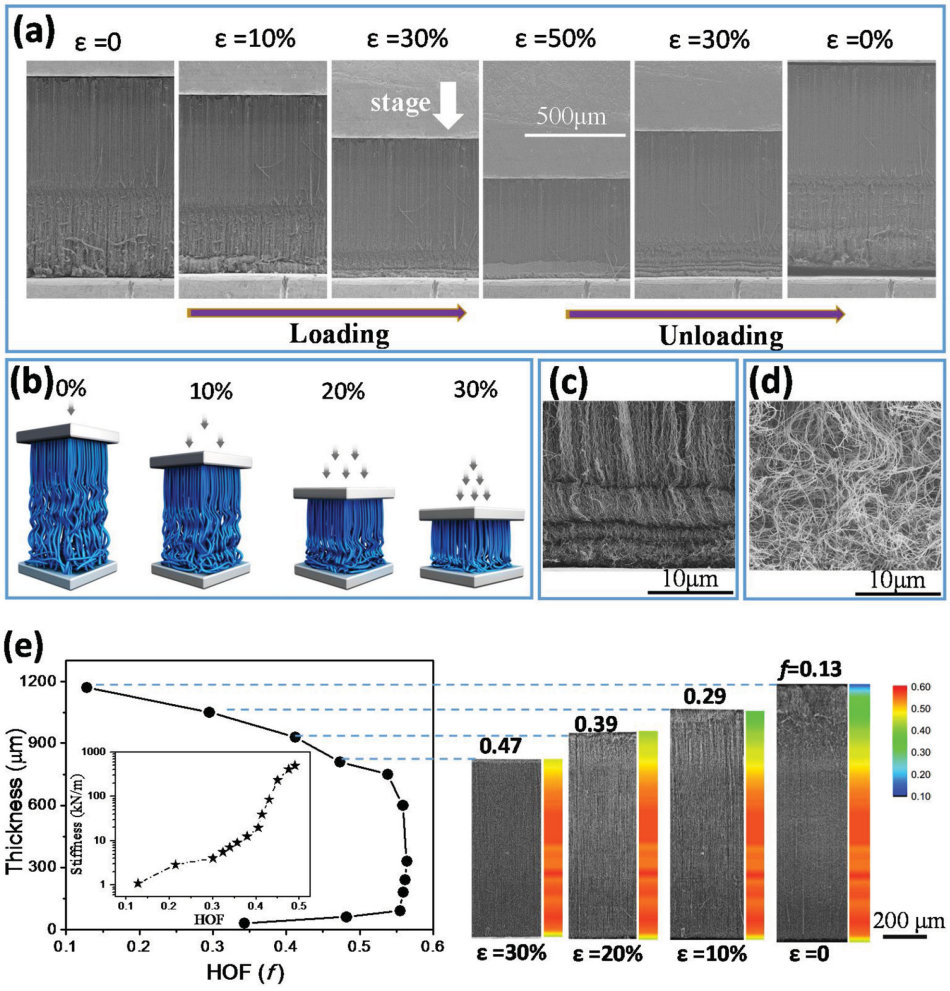

Figure 3. In situ SEM characterization of gradient CNT films under compression cycles. a) SEM images showing the deformation process of a gradient CNTs as the compressive strain gradually increased to 50% and then decreased to 0%. b) Schematic of the deformation behavior of gradient CNTs. c,d) High-magnification SEM images of the bottom (random part) in the gradient under 50% compressive strain and after loading, respectively. e) Structural change of the samples under compression showing the compressed regions of specific f values (f = 0.13, 0.29, 0.39, and 0.47, respectively) in accordance to different strains (ε = 0–30%) and reduced thickness. Inset shows the local stiffness values (derived from DMA) of regions with different f values.

film, resulting in a triple-layer sponge–array-gradient structure (Figures S6 and S7, Supporting Information).

When dichlorobenzene was added, its concentration increase depended on the initial volume of xylene solution (V_0) based on which the rate of change in dichlorobenzene concentration was calculated (see the Experimental Section). Consequently, this rate would influence the f value change per film thickness (so-called transition rate in the gradient structure). At initial xylene solution volumes of 10–50 mL, the f value in all three samples dropped from >0.5 to nearly 0.1, but with different slopes (Figure 2b; Figure S8, Supporting Information). The transition rate was about 0.77 mm^{-1} when using 50 mL xylene solution, and was enhanced to 2.75 mm^{-1} for a lower xylene volume (V_0 = 10 mL). Different transition rates can be clearly observed in gradient samples produced at V_0 = 10 or 50 mL, respectively. SEM images show that both samples have similar f values at the end of gradient structure (also the random part at the bottom) (f = 0.13 and 0.14, respectively) (Figure 2c,d). About 100 μm distance away, the f value increases to 0.37 for the sample synthesized at V_0 = 10 mL (higher transition rate), while f only increases to 0.26 for V_0 = 50 mL.

Mechanical behavior of our gradient CNT films was investigated by in situ SEM characterization. A 1.2 mm thick gradient film was compressed along the thickness direction between two flat stages installed in SEM. A maximum strain of ε = 50% was set for loading and unloading cyclic tests, and snapshots for specific strains (ε = 0%, 10%, 30%, 50%, respectively) were recorded in sequence (**Figure 3**a). Upon loading, the bottom part (random CNTs with lower f value) was compressed first by forming wavy folds to accommodate the compressive strain. During the loading stage until ε = 50%, the film was compressed from the bottom to the middle, with more horizontally collective folds forming and propagating upward.

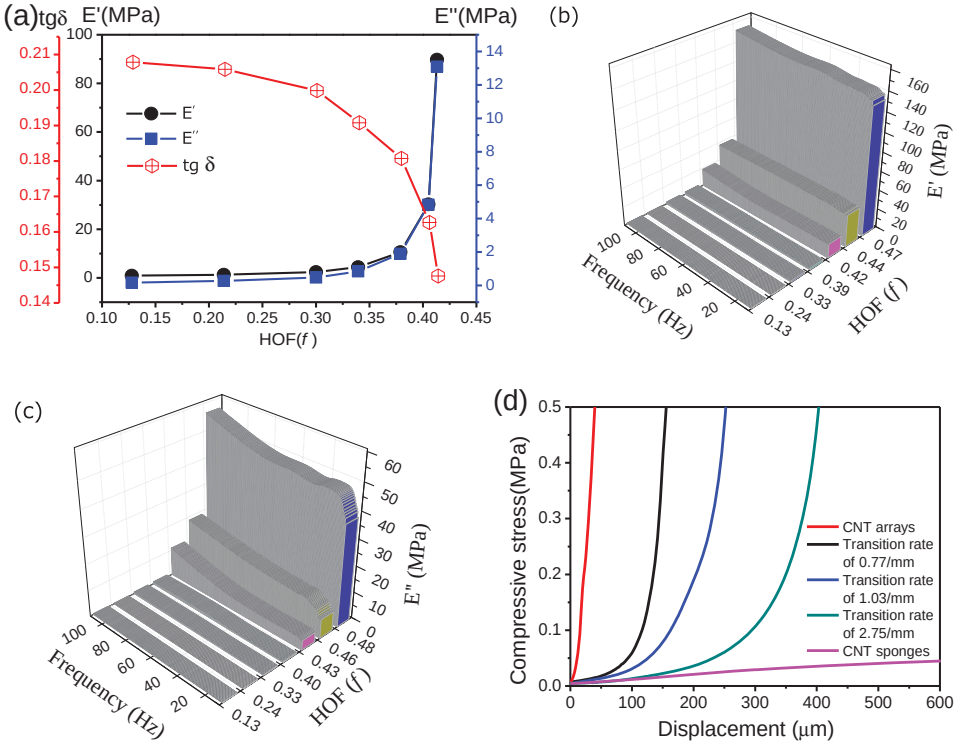

Figure 4. Mechanical Characterization of the gradient CNT films. a) *f* values dependence of the storage modulus (*E'*), loss modulus (*E''*), and damping ratio (tg *δ*) of the gradient CNT films. b,c) Frequency dependence of the storage modulus and loss modulus of the gradient CNTs tested in a frequency range of 0.1–100 Hz at different *f* values. d) Compressive stress-strain curves of CNT arrays, sponges and gradient CNT films with different transition rates of 0.77, 1.03, and 2.75 mm^{-1}.

This observation indicates that CNT arrangements with lower *f* values (more random) tend to deform earlier than those with higher *f* values (aligned array) (illustrated in Figure 3b). Upon unloading, the folds were expanded back into the original random morphology and the film returned to initial thickness (Figure 3c,d), indicating elastic recovery during large-strain deformation.

The compressed (folded) portion with a specific *f* range was correlated with each compressive strain (Figure 3e). At $\varepsilon = 10\%$, the portion corresponding to $f = 0.13–0.29$ has been compressed. When ε increased to 30%, portions with a wider range of *f* values (0.13–0.47) could be compressed while those with high *f* (0.47–0.56) remained straight. The corresponding mechanical properties (stiffness and elastic modulus) could be obtained from dynamic mechanical analysis (DMA) at predefined compressive strains (and *f* values). Our gradient CNT films have stiffness (1.1–494.4 kN m^{-1}) and elastic modulus (0.2–82.3 MPa) spanning over three orders of magnitude for tailored CNT arrangements ($f = 0.13–0.47$) (inset of Figure 3e; Figure S9, Supporting Information). Such stiffness range achievable within a single material free of macroscopic interfaces is greater than that of other artificial graded composites,[7] and is slightly lower than that of heterogeneous composite materials.[3] It was reported that lower density regions of CNT arrays usually tended to buckle before higher density parts,[16,34–37] but here the gradient structure CNT has the same density with the aligned part as measured from macroscopic films with different size. Therefore, the major factor that tailors local mechanical properties as shown here is the Herman's orientation factor, rather than the difference in material density.

Further DMA characterization demonstrated that the viscoelastic properties (storage modulus, loss modulus, and damping ratio) of the CNT films also strongly depended on the arrangement of the CNT. For example, an increase in *f* value results in consistent increase in both moduli (**Figure 4**a). Frequency dependence tests (Figure 4b,c) showed constant viscoelastic properties of the gradient CNT film in a wide range (0.1–100 Hz) at any local region between $f = 0.13–0.54$, indicating excellent reversible deformation and fatigue resistance even in very high frequency, similar to CNT or graphene porous structure.[14,38] In addition, mechanical behavior of gradient CNT films also depended on the transition rate, or how fast the *f* value changed along the thickness. Compressive stress–displacement curves for samples with three transition rates of 0.77, 1.03, and 2.75 mm^{-1} (corresponding to an initial xylene solution volume of 10, 30, and 50 mL, respectively) show quite different behavior during loading (Figure 4d). Pure aligned CNT arrays ($f > 0.5$) appear to be the stiffest sample, with a compressive displacement of only 15.6 μm at 0.1 MPa stress. In comparison, the displacement under the same stress increases to 116.4, 162.8, and 294.5 μm for gradient samples with transition rates of 0.77, 1.03, and 2.75 mm^{-1} , respectively, while pure random CNT sponges show largest deformation.

3. Conclusions

Macroscopic CNT films with controlled gradient structure have been fabricated through a simple CVD process and their mechanical properties investigated. Our CNT films contain a continuous and smooth transition from aligned arrays to completely random distribution, which is distinct from previous CNT-based materials or heterogeneous composites with abrupt interfaces. Local mechanical properties such as stiffness and elastic modulus are determined by the Herman's orientation factor, and span over three orders of magnitude within a single monolithic film. It might be possible to infiltrate or graft specific polymers into these CNT films to make reinforced nanocomposites with gradient microstructure (changing from anisotropic to isotropic gradually) as well as locally tunable mechanical and electrical properties. Gradient CNT structures and composites provide an exciting opportunity in extending applications to those areas where accurate and special gradient of material configuration and property are required.

4. Experimental Section

Synthesis of CNT Blocks with Gradient Structure: CNT films with gradient structures were synthesized by CVD process in a horizontal tubular furnace using ferrocene as catalyst precursor, and a mixture of dichlorobenzene/xylene solution as carbon source. Ferrocene powders were dissolved in dichlorobenzene and xylene to make homogeneous solutions with a concentration of 60 and 20 mg mL^{-1}, respectively. During growth, firstly, the xylene solution was injected into the reaction tube to synthesize aligned CNT arrays at an speed of 0.4 mL min^{-1}. After gowth of 15 minutes, the dichlorobenzene solution was injected into xylene solution at a speed of 0.2 mL min^{-1} (at this moment, the volume of xylene solution was recorded as V_0). At the same time, it formed a uniformly mixed soultion (dichlorobenzene/xylene solution) under rapid stirring, which was then injected as carbon source for growing gradient structures. During this process, the xylene or dichlorobenzene/xylene solution was uninterruptedly injected into reaction tube at the same speed. The CVD system adopted a reaction temperature of 850 °C, and a mixture of carrier gas of argon and hydrogen at flowing rates of 2000 and 300 sccm, respectively.

The concentration of dichlorobenzene in the mixed carbon source solution can be calculated by

$$C_{db} = \frac{V_{db}}{V} = \frac{0.2}{V_0}t \quad (1)$$

where V is the total volume of the mixed solution and t is the growth time when using the mixed solution as carbon source.

Structural Characterization: The microstructure and morphology of gradient CNTs were characterized by SEM (Hitachi S-4800) and TEM (JEM-2010HR). The SEM equiped with a miniaturized compression station were applied to test the in situ morphology of samples at different compressive strains. Mechanical properties were tested by a single-column mechanical testing system (Instron 5943) equipped with a 1 kN load cell and two flat-surface steel compression stages. The size of gradient CNTs for mechanical test is about $10 \times 10 \times 1$ mm^3 (length by width by thickness). Viscoelastic properties were examined by the compression mode Dynamic Mechanical Analyzers (NETZSCH DMA 242c). The tests were carried out at room temperature. Dynamic oscillatory testing was used, where a sinusoidal stress was applied to the samples and a sinusoidal strain was measured.

Herman's Orientation Factor Calculation: HOF, f, has been used to assess the orientation of fiber and nanotube.[20,25,39] Here, we use f value to evaluate the orientation of the CNTs, which was calculated from the standard formulation as defined by

$$f = \frac{1}{2}\left(3\langle\cos^2\phi\rangle - 1\right) \quad (2)$$

$$\langle\cos^2\phi\rangle = \frac{\int_0^{\frac{\pi}{2}} I(\phi)\cos^2\phi\sin\phi d\phi}{\int_0^{\frac{\pi}{2}} I(\phi)\sin^2\phi d\phi} \quad (3)$$

where ϕ is the azimuthal angle between the structural unit vector and the reference dircetion. $I(\phi)$ is the internsity profile as a function of ϕ. $I(\phi)$ is derived from FFT images, which is based on SEM image of the sample at an angle of ϕ. The value of f is equal to 1 for a structure with perfect orientation parallel to reference direction and 0 for randomly oriented samples.

Supporting Information

Supporting Information is available from the Wiley Online Library or from the author.

Acknowledgements

This work was partially supported by Guangdong Natural Science Funds for Distinguished Young Scholar (Grant No. 2014A030306022) and Pearl River S&T Nova Program of Guangzhou (Grant No. 2014J2200066). A. Cao acknowledges financial support from the National Nature Science Foundation of China (Grant No. 51325202).

Received: August 10, 2015
Revised: September 20, 2015
Published online: October 31, 2015

[1] U. G. K. Wegst, H. Bai, E. Saiz, A. P. Tomsia, R. O. Ritchie, *Nat. Mater.* **2015**, *14*, 23.
[2] B. J. F. Bruet, J. Song, M. C. Boyce, C. Ortiz, *Nat. Mater.* **2008**, *7*, 748.
[3] R. Libanori, R. M. Erb, A. Reiser, H. Le Ferrand, M. J. Sueess, R. Spolenak, A. R. Studart, *Nat. Commun.* **2012**, *3*, 1265.
[4] J. D. Fox, J. R. Capadona, P. D. Marasco, S. J. Rowan, *J. Am. Chem. Soc.* **2013**, *135*, 5167.
[5] L. Kesong, J. Lei, *Nano Today* **2011**, *6*, 155.
[6] S. Suresh, *Science* **2001**, *292*, 2447.
[7] X. Li, J. Xie, J. Lipner, X. Yuan, S. Thomopoulos, Y. Xia, *Nano Lett.* **2009**, *9*, 2763.
[8] D. Nuvoli, V. Alzari, J. A. Pojman, V. Sanna, A. Ruiu, D. Sanna, G. Malucelli, A. Mariani, *ACS Appl. Mater. Interfaces* **2015**, *7*, 3600.
[9] A. Y. Cao, P. L. Dickrell, W. G. Sawyer, M. N. Ghasemi-Nejhad, P. M. Ajayan, *Science* **2005**, *310*, 1307.
[10] L. T. Qu, L. M. Dai, M. Stone, Z. H. Xia, Z. L. Wang, *Science* **2008**, *322*, 238.
[11] X. Gui, J. Wei, K. Wang, A. Cao, H. Zhu, Y. Jia, Q. Shu, D. Wu, *Adv. Mater.* **2010**, *22*, 617.
[12] M. B. Bryning, D. E. Milkie, M. F. Islam, L. A. Hough, J. M. Kikkawa, A. G. Yodh, *Adv. Mater.* **2007**, *19*, 661.
[13] H. K. Kyu, O. Youngseok, M. F. Islam, *Nat. Nanotech.* **2012**, *7*, 562.
[14] M. Xu, D. N. Futaba, T. Yamada, M. Yumura, K. Hata, *Science* **2010**, *330*, 1364.
[15] C. Shan, W. Zhao, X. L. Lu, D. J. O'Brien, Y. Li, Z. Cao, A. L. Elias, R. Cruz-Silva, M. Terrones, B. Wei, J. Suhr, *Nano Lett.* **2013**, *13*, 5514.

[16] S. Pathak, N. Mohan, E. Decolvenaere, A. Needleman, M. Bedewy, A. J. Hart, J. R. Greer, *ACS Nano* **2013**, *7*, 8593.
[17] O. Yaglioglu, A. Cao, A. J. Hart, R. Martens, A. H. Slocum, *Adv. Funct. Mater.* **2012**, *22*, 5028.
[18] S. Ozden, C. S. Tiwary, A. H. C. Hart, A. C. Chipara, R. Romero-Aburto, M. F. Rodrigues, J. Taha-Tijerina, R. Vajtai, P. M. Ajayan, *Adv. Mater.* **2015**, *27*, 1842.
[19] D. P. Hashim, N. T. Narayanan, J. M. Romo-Herrera, D. A. Cullen, M. G. Hahm, P. Lezzi, J. R. Suttle, D. Kelkhoff, E. Munoz-Sandoval, S. Ganguli, A. K. Roy, D. J. Smith, R. Vajtai, B. G. Sumpter, V. Meunier, H. Terrones, M. Terrones, P. M. Ajayan, *Sci. Rep.* **2012**, *2*, 363.
[20] M. Xu, D. N. Futaba, M. Yumura, K. Hata, *ACS Nano* **2012**, *6*, 5837.
[21] Y. Zhang, G. Zou, S. K. Doorn, H. Htoon, L. Stan, M. E. Hawley, C. J. Sheehan, Y. Zhu, Q. Jia, *ACS Nano* **2009**, *3*, 2157.
[22] J. R. Raney, R. Y. Wang, C. Daraio, *Carbon* **2013**, *52*, 193.
[23] J. J. Jackson, A. A. Puretzky, K. L. More, C. M. Rouleau, G. Eres, D. B. Geohegan, *ACS Nano* **2010**, *4*, 7573.
[24] M. Bedewy, E. R. Meshot, H. Guo, E. A. Verploegen, W. Lu, A. J. Hart, *J. Phys. Chem. C* **2009**, *113*, 20576.
[25] M. Bedewy, E. R. Meshot, M. J. Reinker, A. J. Hart, *ACS Nano* **2011**, *5*, 8974.
[26] Z. Zeng, X. Gui, Z. Lin, L. Zhang, Y. Jia, A. Cao, Y. Zhu, R. Xiang, T. Wu, Z. Tang, *Adv. Mater.* **2013**, *25*, 1185.
[27] Z. P. Yang, L. J. Ci, J. A. Bur, S. Y. Lin, P. M. Ajayan, *Nano Lett.* **2008**, *8*, 446.
[28] Y. M. Sun, R. B. Sills, X. L. Hu, Z. W. Seh, X. Xiao, H. H. Xu, W. Luo, H. Y. Jin, Y. Xin, T. Q. Li, Z. L. Zhang, J. Zhou, W. Cai, Y. H. Huang, Y. Cui, *Nano Lett.* **2015**, *15*, 3899.
[29] Stéphane Schröder, Comparing Mechanical Properties of Bamboo: Guadua vs Moso, http://www.guaduabamboo.com/guadua/comparing-mechanical-properties-of-bamboo-guadua-vs-moso (accessed: January **2011**).
[30] R. Lv, F. Kang, W. Wang, J. Wei, J. Gu, K. Wang, D. Wu, *Carbon* **2007**, *45*, 1433.
[31] X. C. Gui, Z. Q. Lin, Z. P. Zeng, K. L. Wang, D. H. Wu, Z. K. Tang, *Nanotechnology* **2013**, *24*, 85705.
[32] E. R. Meshot, A. J. Hart, *Appl. Phys. Lett.* **2008**, *92*, 113107.
[33] X. Yang, L. Yuan, V. K. Peterson, A. I. Minett, M. Zhao, N. Kirby, S. Mudie, A. T. Harris, *ACS Appl. Mater. Interfaces* **2013**, *5*, 3063.
[34] R. Theuamaran, E. R. Meshot, C. Daraio, *Carbon* **2015**, *84*, 390.
[35] W. Yoonjin, G. Yuan, M. A. Panzer, S. Dogbe, L. Pan, T. W. Kenny, K. E. Goodson, *Carbon* **2012**, *50*, 347.
[36] M. R. Maschmann, Q. Zhang, F. Du, L. Dai, J. Baur, *Carbon* **2011**, *49*, 386.
[37] M. Bedewy, A. J. Hart, *Nanoscale* **2013**, *5*, 2928.
[38] Y. Wu, N. Yi, L. Huang, T. Zhang, S. Fang, H. Chang, N. Li, J. Oh, J. A. Lee, M. Kozlov, A. C. Chipara, H. Terrones, P. Xiao, G. Long, Y. Huang, F. Zhang, L. Zhang, X. Lepro, C. Haines, M. D. Lima, N. P. Lopez, L. P. Rajukumar, A. L. Elias, S. Feng, S. J. Kim, N. T. Narayanan, P. M. Ajayan, M. Terrones, A. Aliev, P. Chu, Z. Zhang, R. H. Baughman, Y. Chen, *Nat. Commun.* **2015**, *6*, 6141
[39] M. T. Cole, M. Doherty, R. Parmee, P. Dawson, W. I. Milne, *Adv. Opt. Mater.* **2014**, *2*, 929.